

# JOURNAL OF PHARMACEUTICAL ANALYSIS



# GREEN SYNTHESIS OF ZINC OXIDE NANOPARTICLES USING OKRA FRUIT EXTRACT: PHYSICOCHEMICAL CHARACTERIZATION AND EVALUATION OF WOUND HEALING, ANTIOXIDANT, AND CYTOTOXIC ACTIVITIES

# Erdal Ertaș<sup>1\*</sup>, Nurullah Deniz<sup>2</sup>

<sup>1</sup>Department of Food Technology, Vocational School of Technical Sciences, Batman University, 72000 Batman, Turkey.

<sup>2</sup>Graduate Education Institute Student, Batman University, Batman TR-72060, Türkiye \*Corresponding author: Erdal Ertaş, Department of Food Technology, Vocational School of Technical Sciences, Batman University, 72000 Batman, Turkey E-mail:

erdalertas21@gmail.com

#### **Abstract**

Cancer is a leading cause of global mortality, which points to the need for alternative therapies due to the limitations of current chemotherapy, such as low efficacy, toxicity, and drug resistance. Nanotechnology, especially the green synthesis of metal and semiconductor nanoparticles, offers a promising solution with advantages in cost-effectiveness, environmental sustainability, and reduced toxicity. This study investigates the synthesis of zinc oxide nanoparticles (ZnO NPs) via bioreduction of Zn<sup>2+</sup> ions using okra fruit extract (OFE) under rapid, cost-effective, and environmentally benign conditions. OFE-ZnO nanoparticles were characterized by UV-Vis spectroscopy, FTIR, SEM, EDX, XRD, DLS, and zeta potential techniques. UV-Vis analysis for OFE-ZnO nanoparticles showed a surface plasmon resonance peak at 374 nm. In FTIR analysis, a distinct Zn-O stretching vibration was obtained at 618 cm<sup>-1</sup>. SEM images revealed that the nanoparticles were spherical in structure with a homogeneous distribution, while EDX analysis confirmed the presence of zinc. XRD patterns showed high crystallinity and purity, while DLS analysis revealed an average particle size of 141.7 nm, and the zeta potential of these nanoparticles was calculated as -7.42 mV. Antioxidant activity was evaluated using DPPH and ABTS tests, and it was revealed that OFE-ZnO nanoparticles had significant activity at doses of 123.04±2.37 μg/mL and 56.34±1.84 μg/mL, respectively. The MTT assay showed that cytotoxicity resulted in a significant decrease in cell viability in A549 (lung cancer cell line), MDA-MB-231 (breast cancer cell line), SH-SY5Y (neuroblastoma cell line), and L929 (mouse fibroblast cell line) treated with 1000 μg/mL OFE-ZnO nanoparticles, with viability rates ranging from 11.40±4.12% to 16.30±5.66%. Furthermore, wound healing assays revealed better grafting in A549 cells treated with OFE-ZnO nanoparticles compared to cells treated with OFE alone (25.97±3.77%). The findings demonstrate that OFE-ZnO nanoparticles possess significant antioxidant, cytotoxic, and wound-healing properties and have potential as environmentally sustainable nanomaterials for biomedical use.

**Keywords :** Zinc oxide nanoparticles; Okra fruit extract; Green synthesis; Cytotoxicity; Antioxidant activity; Wound healing inhibition

#### 1. Introduction

Cancer continues to be a significant public health problem, one of the diseases with the highest mortality rates worldwide. Due to the limited efficacy of existing chemotherapeutic agents, toxicity issues, and emerging drug resistance, the need for more effective and biocompatible alternative treatment approaches is increasing [1]. In this context, nanotechnology-based approaches offer significant opportunities, particularly for their applications in the biomedical field. Nanotechnology is a burgeoning interdisciplinary field of research focused on nanoparticles (NPs) with dimensions ranging from 1 to 100 nanometers, possessing enhanced properties such as large surface area, high bioavailability, and robust colloidal moiety [2, 3]. Its wide-ranging applications encompass medicine, environmental science, agriculture, and many other disciplines. One of the key advantages of nanotechnology is its ability to significantly increase surface area relative to volume, demonstrating a range of unique properties. Many biologists, chemists, and researchers have observed a significant increase in nanotechnology research due to the unique properties and diverse applications of nanoparticles. Traditionally, NP synthesis has been achieved through physical, chemical, and mechanical methods. However, due to significant drawbacks of these methods, particularly environmental toxicity, cost, high energy consumption, and the use of toxic chemicals, NP production has shifted to biological (green) methods [4-6].

Plant-based nanoparticle synthesis has recently gained attention as an environmentally friendly alternative to traditional chemical and physical methods. This synthesis method offers advantages, particularly in terms of biocompatibility, due to its affordability, scalability, and lack of toxic chemicals. While nanoparticles produced by traditional methods are limited in biological applications due to the toxic chemicals that can remain on their surfaces, nanoparticles synthesized with plant extracts gain more biocompatible and functional properties thanks to the reducing and stabilizing effects of phytomolecules. Furthermore, these phytomolecules exhibit biological activities such as antibacterial, antioxidant, and anticancer, enhancing the therapeutic potential of the synthesized nanoparticles [7, 8].

Recent studies have focused on the synthesis and applications of metal oxide nanoparticles. Among these metal oxide nanoparticles, ZnO NPs are attracting increasing interest due to their exciting properties, a band gap of 3.37 eV, and an excitation binding energy of 60 meV [9]. Furthermore, ZnO NPs have been reported to possess antibacterial, antifungal, and UV-blocking properties. It is a non-toxic n-type semiconductor with high transparency and beneficial photocatalytic properties, all of which have led to its use in the synthesis of ZnO NPs with anticancer, antioxidant, antimicrobial, photocatalytic, and optical properties [10]. There is a significant demand for developing a simple and environmentally friendly method for synthesizing ZnO NPs. Green synthesis of ZnO NPs is a procedure that has attracted considerable attention due to its simplicity, single-step nature, low cost, environmental friendliness, and the absence of any toxic chemicals [11, 12]. Different plant extracts, including leaves, roots, fruits, and flowers are excellent materials for using an easy and safe environmentally friendly method in the scale-up and industrial production of metal and metal oxide NPs [13].

Okra is an important plant that has long been used as a consumable vegetable in various countries, possessing numerous nutritional and therapeutic values. This plant contains proteins, enzymes, vitamins, carbohydrates, tannins, alkaloids, terpenoids, steroids, flavonoids, and

polyphenols. Okra exhibits anticancer, antimicrobial, antidiabetic, and antifungal properties due to its high free radical antioxidant activity. Because the fruit, flower, leaves, and stem of okra contain varying amounts of phytochemicals, their aqueous extracts have been used in the synthesis of various nanoparticles. Various studies have indicated that the phytochemicals contained in okra extracts (e.g., terpenoids, alkaloids, tannins, and flavonoids) play important roles in both the reduction of metal ions and the stabilization of metal and metal oxide nanoparticles [14-16].

In the present study, ZnO NPs were synthesized from okra fruit extract (OFE) via a green synthesis approach. The synthesized nanoparticles were characterized using UV–Vis spectroscopy, FTIR, SEM, EDX, XRD, DLS, and zeta potential analyses. Their antioxidant activities were assessed by DPPH and ABTS assays, while their anticancer effects were evaluated through MTT assay against A549 (human lung carcinoma), MDA-MB-231 (human breast carcinoma), SH-SY5Y (human neuroblastoma), and L929 (normal fibroblast) cell lines. Furthermore, the in vitro wound healing potential of both OFE and OFE-mediated ZnO NPs was investigated in A549 cells.

#### 2. Materials and Methods

#### 2.1 Materials

Zinc sulfate heptahydrate (ZnSO<sub>4</sub>.7H<sub>2</sub>O), 2,2-diphenyl-1-picrylhydrazyl (DPPH), 2,2'-azinobis (3-ethylbenzothiazoline-6-sulfonic acid), methanol, ethanol, Ascorbic acid (AA), 2,6-Ditert-butyl-4-methylphenol (BHT), 2(3)-tert-Butyl-4-methoxyphenol (BHA) and sodium hydroxide (NaOH) were all purchased from Sigma Aldrich (Schnelldorf, Germany) and were of analytical grade and used without any purification. Distilled and sterile deionized water was used throughout the experimental studies.

#### 2.2 Methods

#### 2.2.1 Okra Fruit Collection

Okra fruits were collected in September from the Karaçevre neighborhood of Diyarbakır Çınar district. The fruits were washed first with tap water and then several times with distilled water to remove dust residue at Batman University Food Technology Laboratory. They were then allowed to dry in an oven at 25 °C. The dried okra fruits were ground into powder using an IKA M 20 Universal Grinder and then used in the study.

#### 2.2.2 Preparation of Okra Fruit Extract

5 g of powdered okra fruit was transferred to a 250 mL beaker. 100 mL of deionized water was added and heated at 60 °C on a magnetic stirrer for 30 minutes. After heating, the resulting mixture was cooled to room temperature, and Whatman No. 1 filter paper was used to remove unreacted residue, resulting in a clear solution. The resulting supernatant was stored at 4 °C for use in both characterization and synthesis studies of OFE-ZnO nanoparticles [18].

#### 2.2.3 Green Synthesis of OFE-ZnO Nanoparticles

For the synthesis of OFE-ZnO nanoparticles, a 1 M solution of the solid form of ZnSO<sub>4</sub>.7H<sub>2</sub>O was prepared, and a 50 mM aqueous zinc solution was obtained from this solution for use in the synthesis. 60 mL of okra fruit extract was added dropwise to 240 mL of the prepared 50 mM zinc sulfate heptahydrate solution and stirred continuously at room temperature. 1 hour after the addition of the okra fruit extract, the pH was adjusted to 10 using freshly prepared 2 M NaOH. The solution was then shaken in a 75 °C water bath for 1 hour and then stirred on a magnetic stirrer set at 75 °C for 2 hours. After a white crystalline precipitate formed, the system

was shut down and allowed to cool at room temperature. After cooling, the solution was centrifuged at 6000 rpm for 30 minutes. The white crystalline precipitate collected at the bottom of the centrifuge tube was washed several times with distilled water and then left to dry in an oven set at 50 °C. The product obtained after drying was calcined in a muffle furnace set at 550 °C and then ground to powder in a mortar. The synthesized OFE-ZnO nanoparticles were characterized using various techniques. After characterization, the product was stored in the dark for use in subsequent studies [17, 18].

## 2.3 Characterization

The morphological image of OFE-ZnO nanoparticles was obtained using an SEM device (LEO-EVO 40/Cambridge-England) by placing the powder sample on a carbon tape, while the elemental composition analysis was performed with an energy dispersive X-ray (EDX) using a Bruker-125 eV (Berlin-Germany) coupled with SEM. The resulting nanoparticle solution was then transferred to a quartz cuvette, and after being placed in the cell, absorption maxima were measured between 200 and 600 nm using a UV-visible spectrophotometer (Agilent Cary 60, Santa Clara, United States). After placing some samples of green synthesized OFE-ZnO nanoparticles and powdered okra fruit on a quartz slide, an FTIR spectrum was obtained between 400 and 4000 using an Agilent Cary 630 spectrophotometer (Santa Clara, United States) at room temperature. The purity and crystalline state of OFE-ZnO nanoparticles were determined using powder X-ray diffraction (XRD) (Rigaku-D/Max 2200 Tokyo, Japan) in the  $2\theta$  range of 3–80°. The synthesized OFE-ZnO nanoparticles were dissolved in deionized water by sonication at 25-30 °C for 5 minutes for the determined concentration range. The solution was then placed in a glass cuvette and subjected to DLS and zeta potential analyses between 1 and 100 nm using a dynamic light scattering particle size analyzer (Malvern Zetasizer Nano ZS, Worcestershire, WR14 1XZ, United Kingdom). To prepare the OFE-ZnO nanoparticles at the desired concentration, they were sonicated for 5 minutes at 25-30 °C and dissolved in deionized water.

#### 2.4 Antioxidant activity

## 2.4.1 DPPH• free radical-scavenging activity assay

4 mL of 100 μM DPPH radical solution was added to 1 mL of OFE-ZnO NPs obtained at various concentrations (25, 50, 100, 150, 200, 250 μg/mL). After DPPH addition, the reaction mixture was incubated in the dark at room temperature for 30 minutes, and then absorbance values were measured at 517 nm wavelength with a UV-Vis spectrophotometer [19]. The percentage of DPPH radical scavenging activity and IC<sub>50</sub> values were calculated using the OFE-ZnO nanoparticle concentrations (μg/mL) prepared in the equation below. IC<sub>50</sub> indicates the amount of nanoparticles required to reduce the DPPH radical scavenging concentration by 50%.

% Inhibition (DPPH•) =  $(A_{control} - A_{sample}) / A_{control} \times 100 (A = Absorbance)$ 

## 2.4.2 ABTS<sup>++</sup> radical-scavenging activity assay

ABTS cation radical scavenging activities of OFE-ZnO NPs were carried out using 2,2'-azino-bis(3-ethylbenzothiazoline-6-sulfonic acid) substance [20]. After mixing 1 mL of OFE-ZnO nanoparticle solution prepared at different concentrations with 4 mL of ABTS solution, the resulting mixture was incubated for 30 minutes in the dark at room temperature. The absorbance values of the mixtures obtained after incubation were then read at 734 nm on a UV-Vis spectrophotometer, and the % inhibition values were determined using the equation below,

and the results were expressed as  $IC_{50}$  values. The  $IC_{50}$  value is used to express the amount of nanoparticles required to reduce the ABTS<sup>+</sup> cation removal concentration by 50%.

% Inhibition (ABTS•+) =  $(A_{control} - A_{sample})/A_{control} \times 100 (A = Absorbance)$ 

#### 2.5 Cell Culture

The A549 human lung cancer cell line, the MDA-MB-231 human breast cancer cell line, the SH-SY5Y human neuroblastoma cell line, and the L929 mouse fibroblast cell line, obtained from the American Type Culture Collection (ATCC), were grown in DMEM medium with 10% FBS, 1% penicillin/streptomycin, L-glutamine, and HEPES in 25 cm<sup>2</sup> flasks at 5% CO<sub>2</sub> and 37 °C. When the flasks were 80-90% full, the cells were passaged into new 25 cm<sup>2</sup> and 75 cm<sup>2</sup> flasks to expand the stocks for use in experiments [21].

## 2.6 Cytotoxicity Test

A549, MDA-MB-231, SH-SY5Y, and L929 cells were seeded in 96-well plates at  $5x10^3$  cells per well. To ensure cell adherence to the plate bottom, cells were incubated in a  $CO_2$  incubator for 24 hours. 1, 10, 100, and 1000  $\mu$ g/mL bay leaf extract and nanoparticle A were applied to the cells for 24 hours. 10  $\mu$ L of MTT reagent (5 mg/mL) was added to each well. After 4 hours of incubation, the medium above the cells was aspirated. 100  $\mu$ L of dimethyl sulfoxide was added to each well to dissolve the formazan dye. The absorbance of the resulting color was measured at 570 nm in a microplate reader [22]. The percentage of viable cells was calculated using the following formula:

% Cell Viability =  $(A_{sample}/A_{control})*100$  (A = Absorbance)

# 2.7 Wound Healing Assay

A549 cells were seeded in 12-well plates at 1x10<sup>5</sup> cells per well. To ensure cell adherence to the plate bottom, the cells were incubated for 24 hours in a CO<sub>2</sub> incubator. The exact center of the wells was drawn with a pipette tip from top to bottom to mimic the wound model. The IC<sub>50</sub> dose of OFE and OFE-ZnO NPs was applied to the cells for 24 hours. Images at 0 and 24 hours were captured using an inverted microscope, and wound closure was analyzed using ImageJ. Results were expressed as % wound closure [23].

## 2.8 Statistical Analysis

GraphPad Prism version 9.3.0 for Windows (GraphPad Software, San Diego, California, USA, www.graphpad.com) was used for statistical analysis. The normal Gaussian distribution of the findings was confirmed with the Shapiro-Wilk normality test. Comparisons of the findings were made using one-way analysis of variance (ANOVA) and Tukey's multiple comparison test. Results are presented as mean  $\pm$  SD. P values < 0.05 were considered statistically significant. Significance levels are presented in the figures as follows: \*\*\*\* = P < 0.0001, \*\*\* = P < 0.001, \*\*= P < 0.05

#### 3. Results and Discussion

# 3.1 Characterization of OFE-ZnO Nanoparticles

The synthesized OFE-ZnO nanoparticles were characterized using FTIR, UV-Vis, SEM, EDX, DLS, zeta Potential and XRD analyses, and their images are presented.

## 3.2 FTIR analysis of OFE-ZnO Nanoparticles

Figure. 1 illustrates the findings of FTIR spectroscopic examination of okra fruit extract (OFE) and green-produced OFE-ZnO nanoparticles, examining the functional groups in OFE and their involvement in the reduction and/or stabilization of OFE-ZnO NPs. The FTIR spectrum of

OFE exhibits several absorption bands, signifying the existence of diverse functional groups. The prominent peak at 3265 cm<sup>-1</sup> signifies the stretching vibration of the hydroxyl (O-H) group present in phenolic compounds, which may possess the capacity to decrease Zn<sup>2+</sup> ions [24]. The signal at 2922 cm<sup>-1</sup> signifies C-H stretching in alcohols and alkenes, which may enhance the stability of ZnO nanoparticles [25]. The peaks at 1625 cm<sup>-1</sup> and 1736 cm<sup>-1</sup> are attributed to the C=O stretching of carboxylic acids and esters, while the peak at 1405 cm<sup>-1</sup> is linked to the C=C alkene stretching [26, 27]. The signal at 1237 cm<sup>-1</sup> signifies the existence of polysaccharides and glycosidic linkages, which may contribute to the stabilization of the nanoparticles [28, 29]. The peaks at 924 and 1017 cm<sup>-1</sup> correspond to the C-H vibrations of alkenes and alkynes, whereas the broad peak at 529 cm<sup>-1</sup> signifies the O-H vibrations in phenols and alcohols [30]. In green synthesis, phenolic and carboxylic acid groups diminish Zn<sup>2+</sup> ions, whereas alcohol and ether groups modulate the surface charges of nanoparticles, facilitating their dispersion. The signal at 618 cm<sup>-1</sup> in the FTIR spectrum of OFE-ZnO nanoparticles is attributed to Zn-O stretching, hence validating the effective synthesis of the nanoparticles. Additionally, the peaks at 1628 and 3339 cm<sup>-1</sup> are attributed to carbonyl and hydroxyl groups, which are believed to contribute to the stability of nanoparticles. Thus, the phytochemical constituents of OFE significantly contribute to the decrease of Zn<sup>2+</sup> ions and the stability of ZnO nanoparticles. Functional groups, including phenolic compounds, carboxylic acids, alcohols, esters, and polysaccharides, an engage in reduction processes while stabilizing nanoparticle surfaces, so reducing agglomeration and augmenting biological activity. The alterations in the FTIR spectrum of OFE-ZnO nanoparticles corroborate the involvement of these constituents in this process [31, 32].

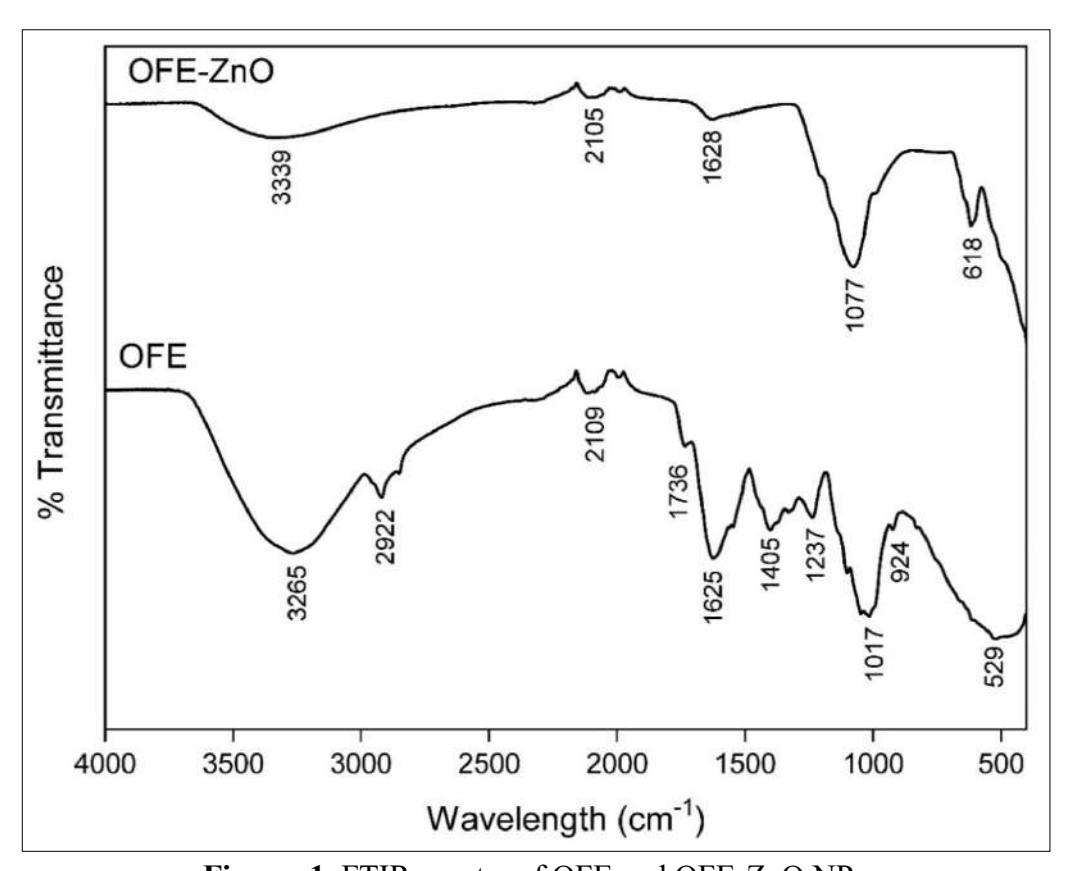


Figure. 1. FTIR spectra of OFE and OFE-ZnO NPs

### 3.2 UV-Vis Analysis of OFE-ZnO Nanoparticles

UV-Vis spectroscopy was performed to confirm the green synthesis of OFE-ZnO NPs in the wavelength region of 200–600 nm at room temperature. As shown in Figure. 2, the UV-Vis absorption spectrum revealed that the maximum absorbance was present at approximately 374 nm, representing the distinctive absorbance peak for ZnO NPs. The surface plasmon resonance (SPR) of ZnO NPs is shown to be the cause of this peak, where the absorption of incident light is a result of the collective emission of free conduction band electrons [33]. Furthermore, no other distinct peaks were observed in the spectrum, confirming the successful synthesis of pure OFE-ZnO NPs. The presence of an absorbance peak at 374 nm is consistent with reports in the literature that ZnO NPs show optical absorption between 340 and 380 nm [34-36].

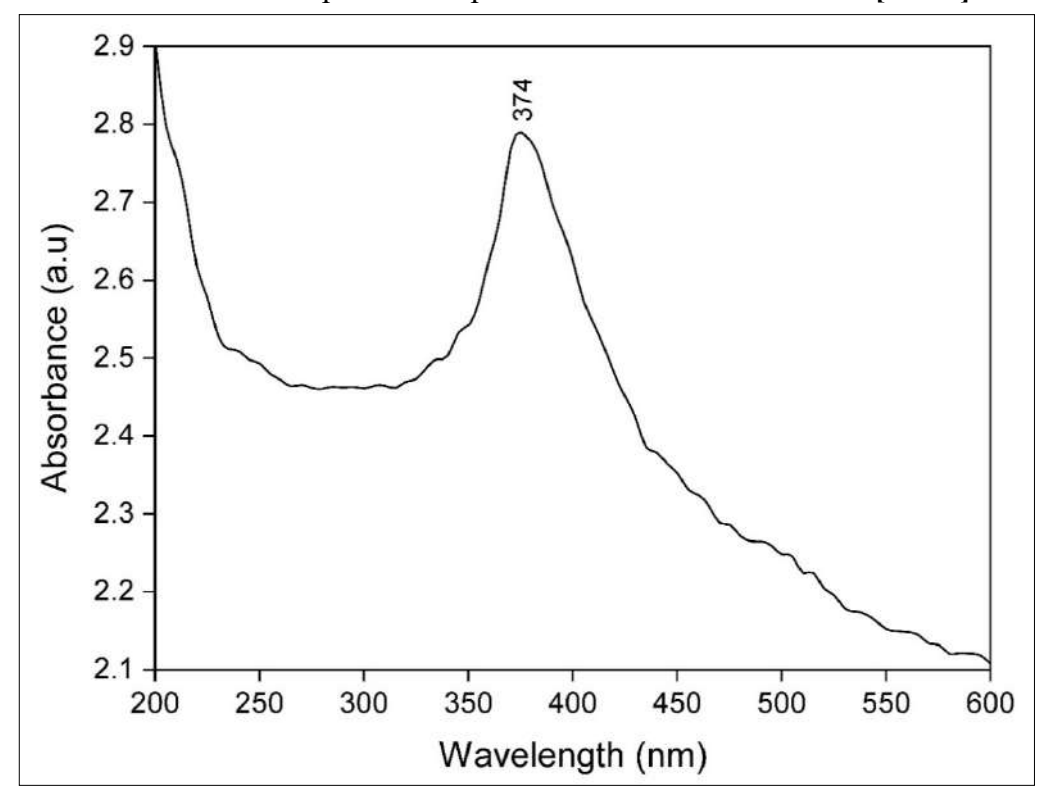


Figure 2. UV-Vis spectrum of OFE-ZnO NPs

## 3.3 SEM Analysis of OFE-ZnO Nanoparticles

The morphological and structural properties of the synthesized OFE-ZnO NPs from OFE were investigated by SEM analysis, and the results are shown in Figure 3. SEM images show that the OFE-ZnO NPs have a distinctly spherical morphology at the nanometer scale and exhibit a uniform distribution. A literature review reveals that the precursor used has a significant effect on the shape and size of the nanoparticles. In particular, when zinc acetate was used as the precursor, the growth of zinc oxide molecules was relatively slow, resulting in the formation of small, spherical nanoparticles. In contrast, when the zinc nitrate precursor was used, the spherical ZnO NPs clustered to form flower-like structures. This clustering is attributed to the electrostatic interactions and polarity of the ZnO NPs. The SEM images in Figure 3 clearly demonstrate that this clustering behavior is a prominent feature observed under these synthesis conditions [17, 37, 38].

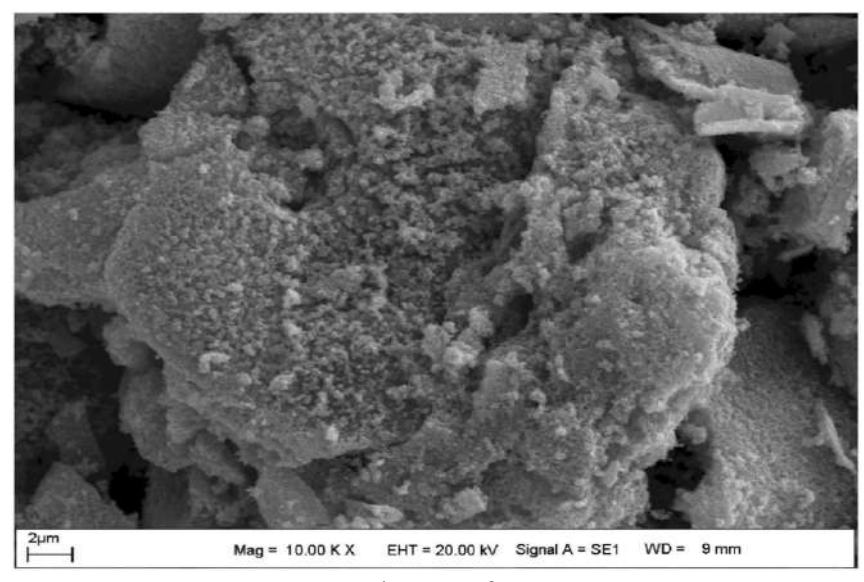


Figure 3. SEM image of OFE-ZnO NPs

## 3.4 EDX Analysis of OFE-ZnO Nanoparticles

The elemental composition of OFE-ZnO NPs was determined by EDX analysis, as shown in Figure 4. The EDX spectrum of OFE-ZnO NPs shows that the elemental mass contents are 50.07% carbon, 22.80% zinc, and 25.87% oxygen. These EDX results further confirm the biosynthesis of OFE-ZnO NPs and the presence of zinc nanoparticles in the oxide form rather than in the pure zinc form. The spectra also indicated that the OFE-ZnO NPs were composed of small amounts of impurities such as sulfur and phosphorus. These impurities may be of biological origin, as found in the plant extract [39].

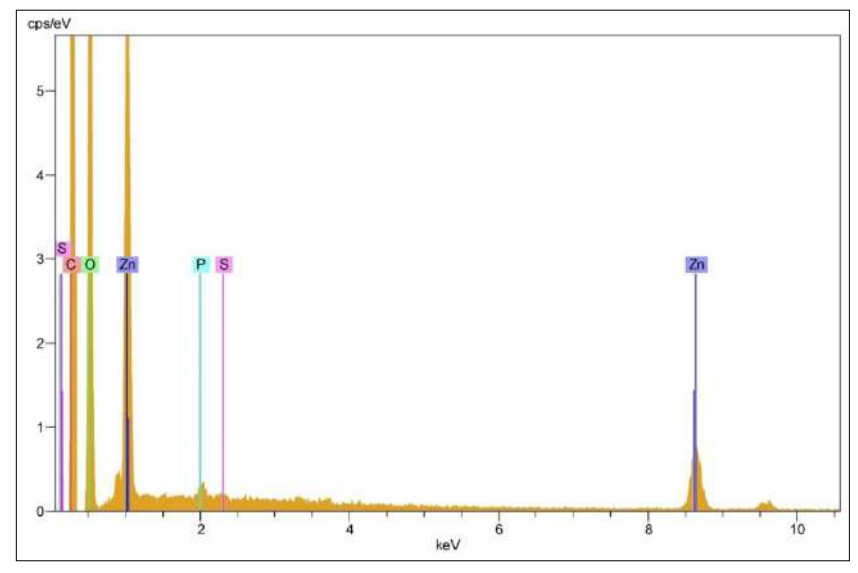


Figure 4. EDX analysis of OFE-ZnO NPs

# 3.5 DLS Analysis of OFE-ZnO Nanoparticles

Particle size was measured using the Dynamic Light Scattering (DLS) method and the Zetasizer device, which are widely used in determining particle size in colloidal solutions. The Zetasizer device has high sensitivity for samples with a molecular weight below 250 Da and can determine the particle sizes of samples suspended in liquid media in the concentration range of

0.00001-40%. Using this technique, the average particle size of OFE-derived ZnO nanoparticles (OFE-ZnO NPs) obtained by the biosynthesis method was analyzed, and the results are presented in **Figure 5.** According to the analysis results, the average hydrodynamic diameter of OFE-ZnO NPs was determined to be approximately 141.7 nm, which indicates the presence of small-scale aggregations **[40, 41].** 

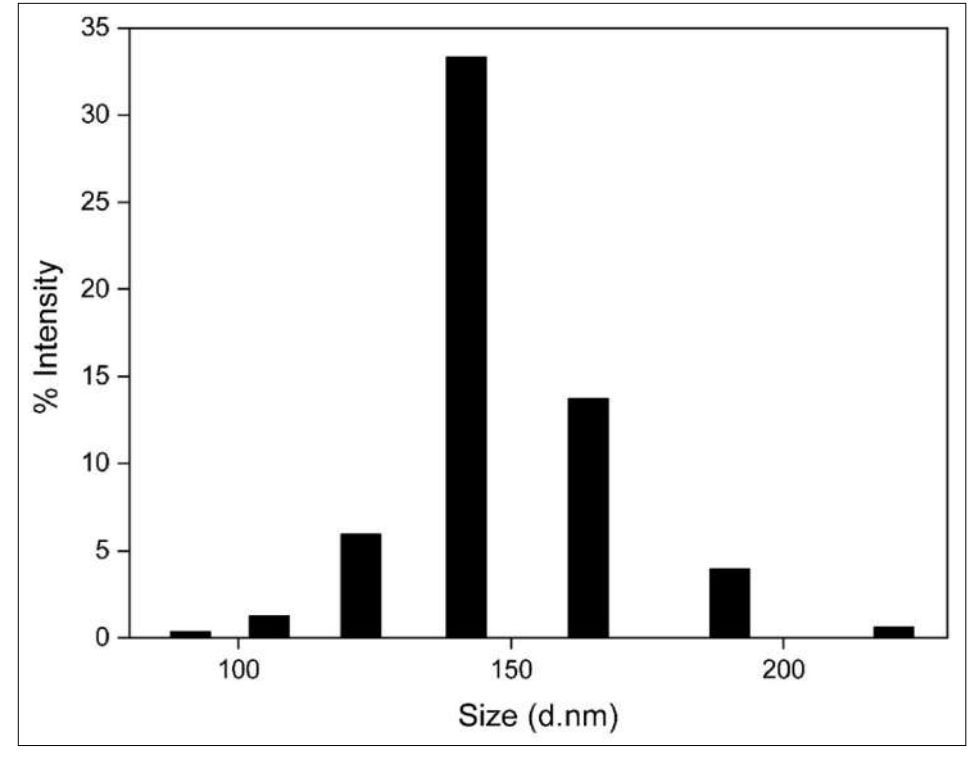


Figure 5. Particle size distribution of OFE-ZnO NPs

## 3.6 Zeta Potential Analysis of OFE-ZnO Nanoparticles

Zeta potential analysis was performed to determine the surface charge of OFE-ZnO NPs biosynthesized using OFE fruit extract [42]. After three replicate measurements of OFE-ZnO NPs obtained using the green synthesis method, the average zeta potential value was found to be -7.42 mV (Figure 6). This result confirms that the biomolecules present in the biosynthesized OFE-ZnO NPs consist mostly of negatively charged groups [43]. The detected negative charge of OFE-ZnO NPs reveals the electrostatic repulsion between the synthesized nanoparticles [44, 45].

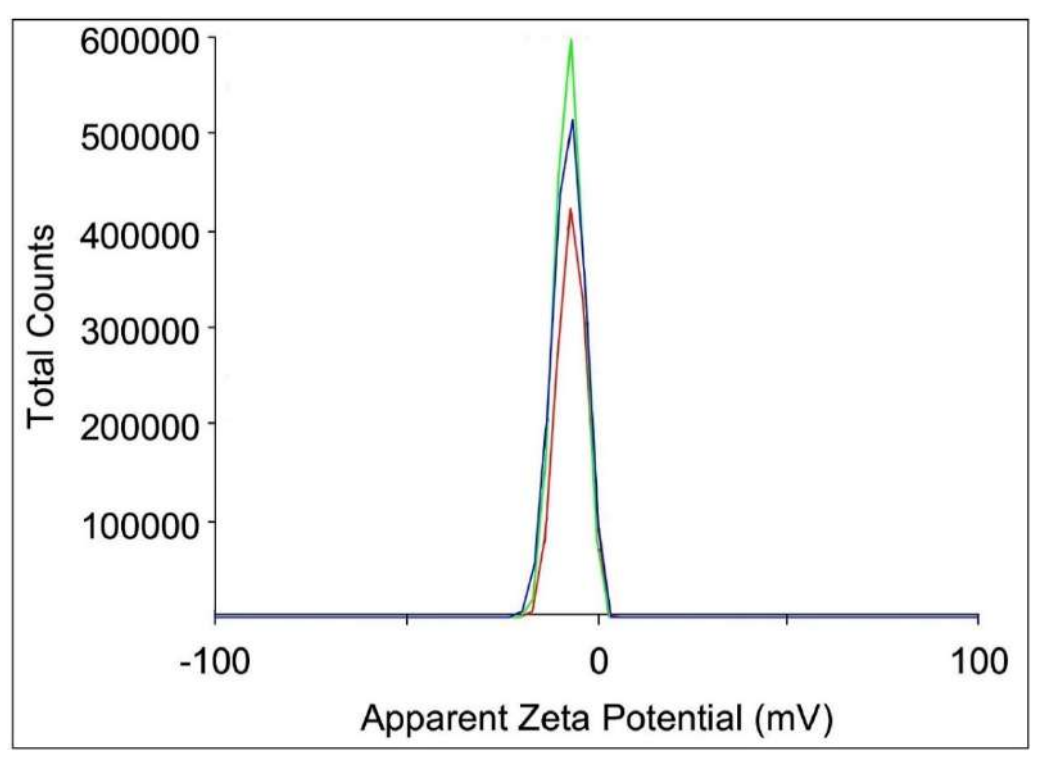


Figure 6. Zeta potential graph of OFE-ZnO NPs

## 3.7 X-ray diffraction (XRD) analysis of OFE-ZnO nanoparticles

Green synthesis of nanoparticles is considered the most cost-effective, biocompatible, and flexible method for nanoparticle synthesis. In vivo biomolecules are highly efficient at reducing metal ions to synthesize functional nanoparticles with superior biocompatibility. XRD analysis was performed on biosynthesized ZnO nanoparticles obtained using okra fruit extract. The presence of fingerprint peaks in the XRD pattern (Figure 7) confirmed the successful formation of OFE-ZnO nanoparticles. When the spectra were examined, seven prominent peaks reflecting the Bragg law were observed at points (100), (002), (101), (102), (110), (103), (112), and (202) with 2θ values of 31.72°, 34.34°, 36.16°, 47.52°, 56.54°, 62.8°, 67.88° and 76.84°, respectively. Furthermore, the obtained XRD pattern corresponds to synthetic ZnO, as indicated by the matching peak positions and the associated Miller indices. The XRD pattern shows good agreement between the experimental data and the reference pattern, with low residual peak intensities (JCPDS-36-1451). This confirms the crystalline structure and phase purity of the synthesized OFE-ZnO nanoparticles, as evidenced by the sharp and narrow peak observed at  $2\theta = 36.16^{\circ}$ . The Debye-Scherrer equation was utilized to estimate the crystal size of the OFE-ZnO nanoparticles. Using the Debye-Scherrer formula, the particle size of the OFE-ZnO nanoparticles was determined to be 36.01 nm [46-49]. Moreover, the absence of any diffraction peak indicating the presence of any impurity demonstrates the purity of the synthesized OFE-ZnO nanoparticles.

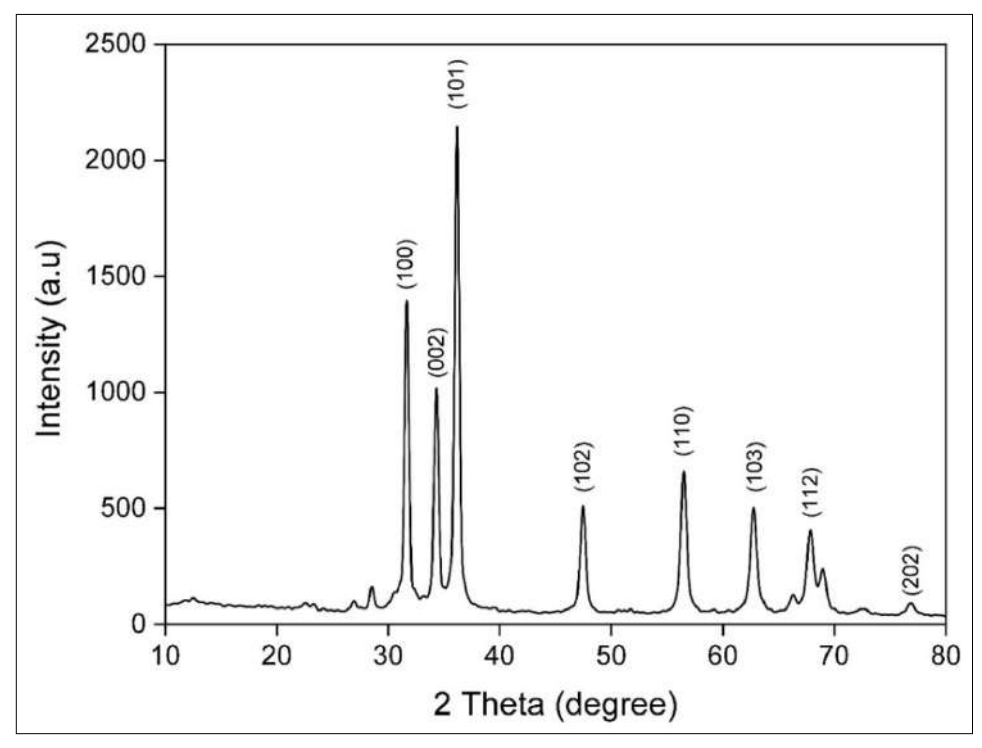


Figure 7. XRD pattern of OFE-ZnO NPs

#### 3.8 Antioxidant Activity

The antioxidant capacity of OFE-ZnO nanoparticles was systematically evaluated using two complementary assays, the DPPH and ABTS++ radical scavenging methods, which rely on distinct reaction mechanisms in **Table1**. Such a dual approach provides a more comprehensive assessment, since the antioxidant response may vary depending on the radical system employed. The IC<sub>50</sub> value obtained from the DPPH assay for OFE-ZnO nanoparticles was  $123.04 \pm 2.37 \,\mu \text{g/mL}$ , indicating a moderate free radical scavenging ability. In general, lower IC<sub>50</sub> values correspond to higher antioxidant potential, as less material is required to neutralize 50% of the radical population. Comparatively, Athmouni et al. reported IC50 values for nine different plant extracts ranging between  $102.31 \pm 2.45$  and  $256.07 \pm 2.07$  µg/mL. This places the antioxidant performance of OFE-ZnO nanoparticles within the effective range observed for natural plant-derived antioxidants, highlighting their potential as a bioactive nanomaterial. In the ABTS assay, the IC50 values were expressed relative to established standards such as ascorbic acid (AA), BHA, and BHT, allowing direct comparison with well-known antioxidants. Literature values, such as the 43.9 µg/mL reported by Adhavan et al., reflect stronger activity than that observed in our study. Nevertheless, the ABTS scavenging capacity of OFE-ZnO nanoparticles remains notable, confirming their ability to effectively interact with the ABTS\* radical cation system The combined results from both assays indicate that OFE-ZnO nanoparticles exhibit significant antioxidant activity, comparable to traditional antioxidants, however with differences based on the examined radical system. The observed differences between DPPH and ABTS values may be attributed to the distinct solubility, polarity, and electron transfer mechanisms involved in the two assays. Such findings underscore the importance of employing multiple evaluation methods to accurately characterize antioxidant activity. Overall, the results suggest that OFE-ZnO nanoparticles have promising potential as antioxidant agents, which may support their further application in biomedical and nutraceutical fields [50,51].

<b>Table 1.</b> Antioxidant activit	y of the ZnO NPs from <i>OFE</i> b	y DPPH', ABTS' assays

	DPPH assay IC <sub>50</sub> (μg/mL)	ABTS <sup>++</sup> assay IC <sub>50</sub> (μg/mL)
OFE-ZnO NPs	123.04±2.37	56.34±1.84
AA	5.76±0.17	2.76±0.12
ВНТ	89.77±1.12	9.16±0.75
ВНА	8.68±0.85	36.04±1.08

<sup>\*</sup>Values expressed are means  $\pm$  SD of three parallel measurements (n=3)

## 3.9 Cytotoxic effects of OFE and OFE-ZnO NPs

Researchers used the A549 human lung cancer cell line, the MDA-MB-231 human breast cancer cell line, and the SH-SY5Y human neuroblastoma cell line to evaluate the cytotoxic effects of OFE-ZnO nanoparticles. The L929 mouse fibroblast cell line was chosen as the healthy. Figure 8A shows morphological images of A549 cells treated with OFE, showing reduced intact and altered cell status compared to the control group. In Figure 8B, the calculated % viability rates of A549, MDA-MB-231, SH-SY5Y, and L929 cells treated with 1000 μg/mL OFE are shown as 52.09±3.73 (p<0.0001), 51.09±3.77 (p<0.0001), 66.90±4.73 (p<0.0001) and 62.52±5.09 (p<0.0001), respectively.

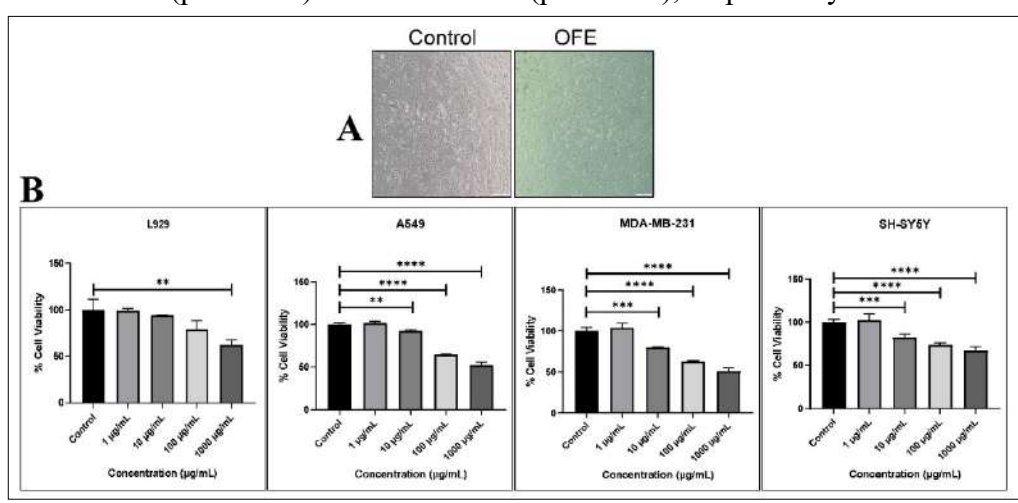


**Figure 8.** Cytotoxic effects of OFE (A) Morphological images of A549 cells treated with IC50 dose of okra extract (B) % viability graphs of A549, MDA-MB-231, SH-SY5Y and L929 cells treated with 1, 10, 100 and 1000  $\mu$ g/mL OFE

Figure 9A shows morphological images of A549 cells treated with OFE-ZnO, showing reduced, intact and altered cell status compared to the control group. In Figure 9B, the calculated % viability rates of A549, MDA-MB-231, SH-SY5Y and L929 cells treated with 1000  $\mu$ g/mL OFE-ZnO are shown as 15.99±1.78 (p<0.0001), 15.80±1.84 (p<0.0001), 16.30±5.66 (p<0.0001) and 11.40±4.12 (p<0.0001), respectively.

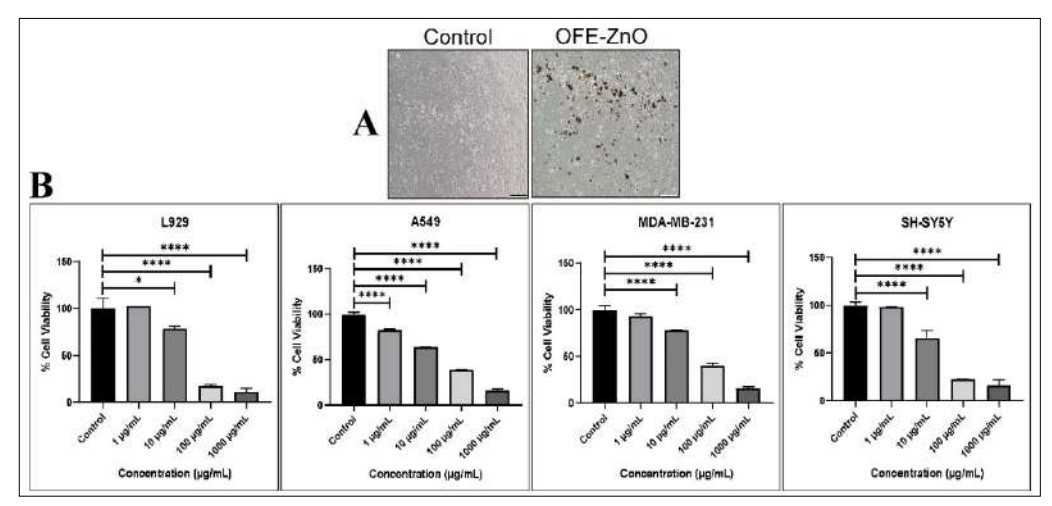


**Figure 9.** Cytotoxic effects of OFE-ZnO NPs (A) Morphological images of A549 cells treated with IC<sub>50</sub> dose of OFE-ZnO NPs (B) % viability graphs of A549, MDA-MB-231, SH-SY5Y, and L929 cells treated with 1, 10, 100, and 1000 μg/mL OFE-ZnO NPs

## 3.10 Migratory effects of OFE and OFE-ZnO nanoparticles

The migrative effects of OFE-ZnO nanoparticles and OFE were tested in the A549 human lung cancer cell line (Figure 10A). The wound closure rates of A549 cells treated with the IC50 dose of OFE and OFE-ZnO nanoparticles were calculated to be 25.97±3.77% (p<0.0001) and 31.69±3.35% (p<0.0001), respectively, when compared to the control group (Figure 10B).

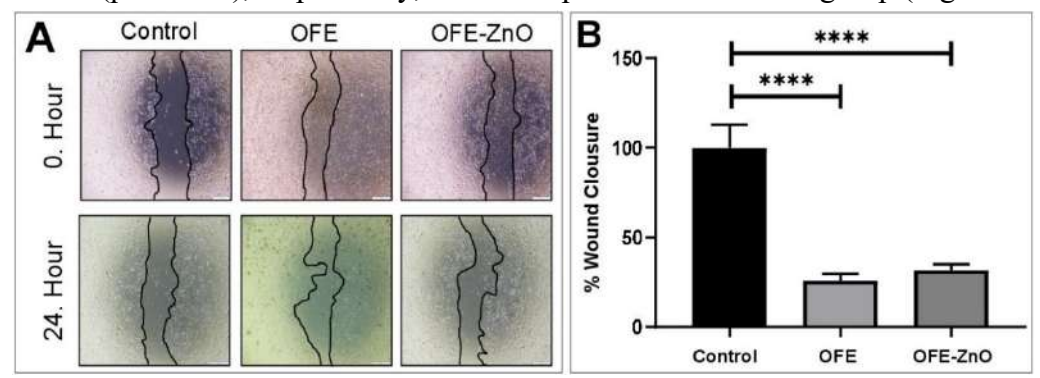


**Figure 10.** Migratory effects of OFE and OFE-ZnO NPs (A) Wound healing of A549 cells treated with IC<sub>50</sub> dose of OFE and OFE-ZnO NPs (B) The wound closure percentage graph of A549 cells treated with OFE and OFE-ZnO NPs

#### 4. Conclusions

OFE-ZnO NPs were synthesized using okra fruit extract (OFE) via the bioreduction method based on green chemistry principles. The synthesized OFE-ZnO nanoparticles were comprehensively characterized by UV-Vis, FTIR, SEM, EDX, XRD, DLS, and zeta potential analyses. UV-Vis spectroscopy showed that OFE-ZnO nanoparticles had a prominent surface plasmon resonance (SPR) band at 374 nm. The FTIR spectrum revealed that the characteristic vibration peak of OFE-ZnO NPs was located at 618 cm<sup>-1</sup>. SEM analysis indicated that the nanoparticles were spherical, uniformly distributed, and in the nanosize range. EDX analysis confirmed the presence of the zinc element, and XRD results demonstrated the high crystalline structure and purity of the nanoparticles. The average particle size was determined to be 141.7 nm, and zeta potential measurements were determined to be -7.42 mV. Antioxidant activity

was assessed using DPPH and ABTS assays. OFE-ZnO nanoparticles demonstrated activity at a concentration of 123.04±2.37 µg/mL in the DPPH assay and 56.34±1.84 µg/mL in the ABTS assay. Ascorbic acid (AA), butylhydroxytoluene (BHT), and butylhydroxyanisole (BHA), used as controls, were compared as known antioxidants. In vitro cytotoxicity tests revealed that OFE and OFE-ZnO NPs exhibited significant cytotoxic effects on lung cancer A549, breast cancer MDA-MB-231, neuroblastoma SH-SY5Y, and mouse fibroblast L929 cell lines. Additionally, the beneficial effects of OFE and OFE-ZnO NPs on wound healing in A549 cells were observed. These findings highlight the growing interest in ZnO nanoparticles derived from plant extracts due to their eco-friendly nature, low toxicity, biocompatibility, costeffectiveness, and sustainability. Their unique optical and chemical properties make them suitable for a wide range of applications, including optics, electronics, food packaging, and biomedical sectors. The beneficial characteristics of green chemistry can enhance the effectiveness of synthetically produced nanoparticles, thereby promoting the development of new therapeutic strategies. Recent studies suggest that the continuous advancements in biosynthesized ZnO nanoparticles are expected to provide significant advantages in medicine, particularly in cancer treatment and wound healing processes, with ZnONPs poised to offer increasingly promising prospects in this field.

**Acknowledgements** This project is financially supported by the Batman University Research Fund (BTÜBAP, Project No. BTÜBAP-2025-YL-08).

## **Authorship Contribution Statement**

E.E. conceived the study, supervised the project, and wrote the manuscript. N.D. performed the synthesis experiments. All authors reviewed and approved the final version of the manuscript.

#### **Funding**

No financial support is relevant to this study.

## **Data availability**

No datasets were generated or analyzed during the current study.

#### **Declarations**

## **Ethical approval**

Not applicable.

## **Consent for publication**

Not applicable.

## **Competing interests**

The authors declare no competing interests.

#### References

- 1. Chai Y, Shi Y (2025) The role of genetics and epigenetics in breast cancer: A comprehensive review of metastasis, risk factors, and future perspectives. J. Pharm. Anal: 101268.
- 2. Parimi DS, Gupta Y, Marpu S, Bhatt CS, Bollu TK, et al. (2022) Nanomagnet-facilitated pharmaco-compatibility for cancer diagnostics: Underlying risks and the emergence of ultrasmall nanomagnets. J. Pharm. Anal. 12: 365-379.
- 3. Das S, Langbang L, Haque M, Belwal VK, Aguan K, et al.(2021) Biocompatible silver nanoparticles: An investigation into their protein binding efficacies, anti-bacterial effects, and cell cytotoxicity studies, J. Pharm. Anal. 11: 422-434.

- 4. Chandrasekaran R, Yadav SA, Sivaperumal S(2020) Phytosynthesis and characterization of copper oxide nanoparticles using the aqueous extract of *Beta vulgaris L* and evaluation of their antibacterial and anticancer activities. J. Clust. Sci. 31: 221-230.
- 5. Lahiri D, Nag M, Sheikh HI,Sarkar T, Edinur HA, et al. (2021) Microbiologically-synthesized nanoparticles and their role in silencing the biofilm signaling cascade. Front. Microbiol 12: 636588.
- 6. Talebian S, Shahnavaz B, Nejabat M, Abolhassani Y, Rassouli FB (2023) Bacterial-mediated synthesis and characterization of copper oxide nanoparticles with antibacterial, antioxidant, and anticancer potentials. Front. Bioeng. Biotechnol 11: 1140010.
- 7. Khan SA, Shahid S, Lee CS (2020) Green synthesis of gold and silver nanoparticles using leaf extract of *Clerodendrum inerme*: characterization, antimicrobial, and antioxidant activities. Biomolecules, 10: 835.
- 8. Khan SA, Shahid S, Hanif S, Almoallim HS, Alharbi SA, et al.(2021) Green synthesis of chromium oxide nanoparticles for antibacterial, antioxidant, anticancer, and biocompatibility activities. Int. J. Mol. Sci. 22: 502.
- 9. Mahalakshmi S, Hema N, Vijaya PP (2020) In vitro biocompatibility and antimicrobial activities of zinc oxide nanoparticles (ZnO NPs) prepared by chemical and green synthetic route—a comparative study. Bionanosci. 10:112-121.
- 10. Elgazzar E, Ayoub HA, El-Wahab ZA, Mostafa WA (2023) Integration of ZnO nanorods with silver ions by a facile co-precipitation for antimicrobial, larvicidal, and ovicidal activity. BMC Biotechnol. 23: 23.
- 11. Abbes N, Bekri I, Cheng M, Sejri N, Cheikhrouhou M, et al.(2022) Green synthesis and characterization of zinc oxide nanoparticles using mulberry fruit and their antioxidant activity, Mater. Sci. 28: 144-150.
- 12. Alahmdi MI, Khasim S, Vanaraj S, Panneerselvam C, Mahmoud MAA, et al.(2022) Green nanoarchitectonics of ZnO nanoparticles from *Clitoria ternatea* flower extract for in vitro anticancer and antibacterial activity: inhibits MCF-7 cell proliferation via intrinsic apoptotic pathway. J. Inorg. Organomet. Polym. Mater. 32: 2146-2159.
- 13. Muddapur UM, Alshehri S, Ghoneim MM, Mahnashi MH, Alshahrani MA, et al.(2022) Plant-based synthesis of gold nanoparticles and theranostic applications: a review. Molecules 27: 1391.
- 14. Kwok CTK, Ng YF, Chan HTL, Chan SW (2025) An overview of the current scientific evidence on the biological properties of *Abelmoschus esculentus* (L.) Moench (Okra), Foods. 14: 177.
- 15. Zhu XM, Xu R, Wang H, Chen JY, Tu ZC (2020) Structural properties, bioactivities, and applications of polysaccharides from Okra [*Abelmoschus esculentus* (L.) Moench]: A review. J. Agric. Food. Chem. 68: 14091-14103.
- 16. Woumbo CY, Kuate D, Metue Tamo DG, Womeni HM (2022) Antioxidant and antidiabetic activities of a polyphenol rich extract obtained from *Abelmoschus esculentus* (okra) seeds using optimized conditions in microwave-assisted extraction (MAE). Front. Nutr. 9: 1030385.
- 17. Moalwi A, Kamat K, Muddapur UM, Aldoah B, AlWadai HH, et al.(2024) Green synthesis of zinc oxide nanoparticles from *Wodyetia bifurcata* fruit peel extract: multifaceted potential in wound healing, antimicrobial, antioxidant, and anticancer applications. Front. Pharmacol. 15: 1435222.

- 18. İpek P, Baran MF, Hatipoğlu A, Baran A(2024) Anticancer Activities of Zinc Oxide Nanoparticles (ZnO NPs) Synthesized from *Mentha longifolia* L. Leaf Extract. J.I.S.T. 14: 107-114.
- 19. Blois MS (1958) Antioxidant determinations by the use of a stable free radical. Nature 181: 1199–1200.
- 20. ReeM BOFE JY, Jung JH, Shin TJ (1999) A new copolymerization process leading to poly (propylene carbonate) with a highly enhanced yield from carbon dioxide and propylene oxide. J. Polym. Sci. Polym. Chem. 37: 1863–1876.
- 21. K Şendal, M Üstün Özgür, E Ortadoğulu Sucu, MB Findik, Ö Erdoğan,et al.(2025) Investigation of antibacterial and anticancer activities of biosynthesized metal-doped and undoped zinc oxide nanoparticles, Biotechnol. Appl. Biochem. 72: 586-609.
- 22. Erdoğan Ö, Paşa S, Demirbolat GM, Birtekocak F, Abbak M, et al.(2025) Synthesis, characterization, and anticarcinogenic potent of green-synthesized zinc oxide nanoparticles via *Citrus aurantium* aqueous peel extract. Inorg. Nano-Met. Chem. 55: 67-75.
- 23. Aytar M, Boncooğlu RY, Erdoğan Ö, Başbülbül G, Öztürk B (2024) Antioxidant, cytotoxicity, antimicrobial, wound healing potentials and LC-MS/MS analysis of water extract of *Rhus coriaria* L. (sumak) leaves. Food Biosci. 60: 104400.
- 24. Patel RV, Yadav A (2022) Photocatalytic MIL101 (Fe)/ZnO chitosan composites for adsorptive removal of tetracycline antibiotics from the aqueous stream, J. Mol. Struct. 1252: 132128.
- 25. Martono Y, RohmanA (2019) Quantitative Analysis of Stevioside and Rebaudioside A in *Steviarebaudiana* Leaves Using Infrared Spectroscopy and Multivariate Calibration. Int. J. Appl. Pharm 11: 38-42.
- 26. Happy A, Soumya M, Kumar SV, Rajeshkumar S, Sheba RD, et al. (2019) Phyto-assisted synthesis of zinc oxide nanoparticles using *Cassia alata* and its antibacterial activity against *Escherichia coli*. Biochem. Biophys. Rep. 17: 208-211.
- 27. Sadeghi B, Mohammadzadeh M, Babakhani B (2015) Green synthesis of gold nanoparticles using *Stevia rebaudiana* leaf extracts: Characterization and their stability. J. Photochem. Photobiol. B: Biol. 148: 101-106.
- 28. Naziruddin MA, Kian LK, Jawaid M, Fouad H, Sanny M, et al.(2023) Sage biomass powders by supercritical fluid extraction and hydro-distillation techniques: a comparative study of biological and chemical properties, Biomass. Convers. Biorefin. 13: 13091-13101.
- 29. Essa HL, Abdelfattah MS, Marzouk AS, Guirguis HA,. El-Sayed MM (2020) Nanoformulations of copper species coated with sulfated polysaccharide extracts and assessment of their phytotoxicity on wheat (*Triticum aestivum L*.) seedlings in seed germination, foliar and soil applications. Appl. Sci. 10: 6302.
- 30. Saleh SS, El-Shayeb NS(2020) Impact of Spirulina platensis and Stevia rebaudiana on growth and essential oil production of basil *Ocimum citriodorum*. J. Agric. Rural. Res. 3: 36-45.
- 31. Shanmugarathinam A, Elamaran N, Kirubakaran D, Irulappan GB, Baig AA, et al.(2025) Sustainable synthesis of zinc oxide nanoparticles from *Vicoa indica* leaf extract: Characterization and evaluation of antibacterial, antioxidant, and anticancer properties. Biomed. Mater. Devices: 1-16.

- 32. Redjili S,Ghodbane H, Tahraoui H, Abdelouahed L, Chebli D, et al. (2025) Green Innovation: Multifunctional Zinc Oxide Nanoparticles Synthesized Using *Quercus robur* for Photocatalytic Performance, Environmental, and Antimicrobial Applications. Catalysts. 15: 256.
- 33. Narayana A, Bhat SA, Fathima A, Lokesh SV, Surya SG, et al.(2020) Green and low-cost synthesis of zinc oxide nanoparticles and their application in transistor-based carbon monoxide sensing. RSC Adv. 10: 13532-13542.
- 34. El Golli A, Contreras S, Dridi CJSR (2023) Bio-synthesized ZnO nanoparticles and sunlight-driven photocatalysis for environmentally friendly and sustainable route of synthetic petroleum refinery wastewater treatment. Sci. Rep. 13: 20809.
- 35. Yashni G, Al-Gheethi A, Mohamed RMSR, Dai-Viet NV, Al-Kahtani AA, et al.(2021) Bio-inspired ZnO NPs synthesized from *Citrus sinensis* peels extract for Congo red removal from textile wastewater via photocatalysis: Optimization, mechanisms, techno-economic analysis. Chemosphere 281: 130661.
- 36. Mongy Y, Shalaby T (2024) Green synthesis of zinc oxide nanoparticles using *Rhus coriaria* extract and their anticancer activity against triple-negative breast cancer cells. Sci. Rep. 14: 13470.
- 37. Fakhari S, Jamzad M, Kabiri Fard H (2019) Green synthesis of zinc oxide nanoparticles: a comparison. Green. Chem. Lett. Rev. 12: 19-24.
- 38. Raut SK, Mondal P, Parameswaran B, Sarkar S, Dey P, et al. (2021) Self-healable ultrahydrophobic modified bio-based elastomer using Diels-Alder 'click chemistry'. Eur. Polym. J. 146: 110204.
- 39. Khalil M, Alqahtany FZ (2020) Comparative studies of the synthesis and physical characterization of ZnO nanoparticles using *Nerium oleander* flower extract and chemical methods. J. Inorg. Organomet. Polym. Mater. 30: 3750-3760.
- 40. Abdelbaky AS, Mohamed AM, Sharaky M, Mohamed NA, Diab YM (2023) Green approach for the synthesis of ZnO nanoparticles using Cymbopogon citratus aqueous leaf extract: characterization and evaluation of their biological activities, Chem. Biol. Technol. Agric 10: 63.
- 41. AA Alyamani, S Albukhaty, S Aloufi, FA AlMalki, H Al-Karagoly, etal.(2021) Green fabrication of zinc oxide nanoparticles using Phlomis leaf extract: characterization and in vitro evaluation of cytotoxicity and antibacterial properties. Molecules. 26: 6140.
- 42. Faisal S, Jan H, Shah SA, Shah S, Khan A, et al. (2021) Green synthesis of zinc oxide (ZnO) nanoparticles using aqueous fruit extracts of *Myristica fragrans*: their characterizations and biological and environmental applications. ACS Omega. 6: 9709-9722.
- 43. Barzinjy AA, Azeez HH (2020) Green synthesis and characterization of zinc oxide nanoparticles using *Eucalyptus globulus Labill*. leaf extract and zinc nitrate hexahydrate salt. SN Appl. Sci. 2: 991.
- 44. Al-Kordy HM, Sabry SA, ME Mabrouk (2021) Statistical optimization of experimental parameters for extracellular synthesis of zinc oxide nanoparticles by a novel *Haloalaliphilic Alkalibacillus sp.* W7. Sci. Rep. 11: 10924.
- 45. Yassin MT, Mostaf AAF, Al-Askar AA, Al-Otibi FO (2022) Facile green synthesis of zinc oxide nanoparticles with potential synergistic activity with common antifungal agents against multidrug-resistant candidal strains. Crystals. 12: 774.

- 46. Almuhayawi MS, Alruhaili MH, Soliman MK, Tarabulsi MK, Ashy RA, et al.(2024) Investigating the in vitro antibacterial, antibiofilm, antioxidant, anticancer and antiviral activities of zinc oxide nanoparticles biofabricated from *Cassia javanica*. Plos. One. 19: e0310927.
- 47. Alghamdi RA, Al-Zahrani MH, Altarjami LR, Abdulmonem W Al, Samir N, et al.(2023) Biogenic Zinc oxide nanoparticles from Celosia argentea: toward improved antioxidant, antibacterial, and anticancer activities. Front. Bioeng. Biotechnol. 11: 1283898.
- 48. Azim Z, Singh NB, Khare S, Singh A, Amist N, et al.(2022) Green synthesis of zinc oxide nanoparticles using *Vernonia cinerea* leaf extract and evaluation as nano-nutrient on the growth and development of tomato seedling. Plant. Nano. Biology. 2: 100011.
- 49. S Faisal, H Jan, SA Shah, S Shah, A Khan, et al. (2021) Green synthesis of zinc oxide (ZnO) nanoparticles using aqueous fruit extracts of Myristica fragrans: their characterizations and biological and environmental applications. ACS Omega. 6: 9709-9722.
- 50. Athmouni K, Belghith T, Fek A El, Ayadi H (2016) Phytochemical composition and antioxidant activity of extracts of some medicinal plants in Tunisia. Int. J. Pharmacol. Toxicol. 4: 159-168.
- 51. Adhavan R, Selvam K, Prakash P, Manimegalai P, Kirubakaran D, et al. (2024) Bioefficacy of Zinc oxide nanoparticle synthesis and their Biological, Environmental applications from Eranthemum roseum. Toxicol. Rep. 13:101758.